Magnetic effects on nonlinear mechanical properties of a suspended carbon nanotube

A. Nocera,[1,2] C. A. Perroni,[3,4] V. Marigliano Ramaglia,[1,4] G. Cantele,[3] and V. Cataudella[3,4]
[1]*CNISM, UdR Napoli Università, Monte SantAngelo, Via Cintia, I-80126 Napoli, Italy*
[2]*Dipartimento di Fisica E. Amaldi, Università di Roma Tre, Via della Vasca Navale 84, I-00146 Roma, Italy*
[3]*CNR-SPIN, Monte SantAngelo, Via Cintia, I-80126 Napoli, Italy*
[4]*Università degli Studi di Napoli Federico II, Complesso Universitario Monte Sant'Angelo, Via Cintia, I-80126 Napoli, Italy*
(Received 29 December 2012; published 25 April 2013)

We propose a microscopic model for a nanoelectromechanical system made by a radio-frequency driven suspended carbon nanotube (CNT) in the presence of an external magnetic field perpendicular to the current. As a main result, we show that, when the device is driven far from equilibrium, one can tune the CNT mechanical properties by varying the external magnetic field. Indeed, the magnetic field affects the CNT bending mode dynamics inducing an enhanced damping as well as a noise term due to the electronic phase fluctuations. The quality factor, as observed experimentally, exhibits a quadratic dependence on external magnetic field strength. Finally, CNT resonance frequencies as a function of gate voltage acquire, increasing the magnetic field strength, a peculiar dip-peak structure that should be experimentally observed.

DOI: 10.1103/PhysRevB.87.155435 PACS number(s): 85.65.+h, 63.22.Gh, 73.63.−b, 85.85.+j

I. INTRODUCTION

Nanoelectromechanical Systems (NEMS) made of suspended carbon nanotubes (CNTs) have received increasing attention recently.[1–8] These devices are ideal for NEMS applications due to the extreme mechanical properties of CNTs (low mass density and a high Young's modulus), resulting in a wide range of resonance frequencies for the fundamental bending mode vibration [from MHz up to GHz (Ref. 9) range]. For instance, this has made it possible to operate with ultrahigh frequency devices and therefore explore the quantum ground state of a macroscopic object.[10]

On the other hand, CNT-based electromechanical devices working in the adiabatic regime (resonator frequencies in the MHz range compared to an electronic hopping frequency from the leads of the order of tens of GHz) have attracted great interest due to the extremely large quality factors ($Q > 10^5$) attainable.[2,3,11] Large quality factors allow one to tune CNT mechanical properties, e.g., the resonance frequency of the bending mode, by adjusting electronic parameters such as gate and bias voltages with a resolution of a few MHz.[2,12] Furthermore, it has been recently demonstrated that the application of a static magnetic field perpendicular to the CNT device can be used as another useful tool for tuning its mechanical characteristics,[1] as the electronic current flow through the CNT beam is affected by the Lorentz force.

The properties mentioned above are due to the fact that suspended CNTs, at cryogenic temperatures, behave as quantum dots[13–15] with a strong interplay between single-electron tunneling and bending mode mechanical motion.[2,12,16–19] This means that the electronic current is very sensitive to the CNT bending mode dynamics and can be used as a quantum (due to the intrinsic quantum nature of the charge carriers) mean for studying its mechanical characteristics.

Motivated by recent experiments,[1,12] in this paper we study a general model describing the mechanical properties of a radio-frequency driven suspended CNT-based NEMS in the presence of a magnetic field transverse to the CNT oscillation plane. To study this system, we employ the same model adopted by some of us in Ref. 16. There we showed that the effects of damping, spring stiffening, and softening, and nonlinearity observed in CNT-based NEMS devices in the absence of a magnetic field[2,3,20] can be understood in terms of a very simple schematization for the CNT device: the electronic part is described by a single electronic level[16,21] coupled to two metallic leads, while the mechanical part is described by a single vibrational degree of freedom describing the bending mode.[22] The interaction between electronic and mechanical parts is described by means of a simple charge-displacement coupling.[16,21] Due to a very large separation between slow vibrational and fast electronic time scales, it can be shown that the CNT bending mode mechanical dynamics is ruled by a classical Langevin equation.[21,24–30] In other terms, the vibrating CNT can be fruitful described as an effective harmonic spring embedded in a nonequilibrium environment consisting of both the nanotube itself and by the macroscopic voltage-biased leads. Furthermore, the external antenna effects are included introducing a forcing term in the Langevin equation. In Ref. 16, we explored the nonlinear vibrational regime of the CNT dynamics, showing that nonlinear effects are obtained by applying large external antenna amplitudes due to the dynamical effects. We were also able to reproduce qualitatively, in the linear response regime, the shape of the CNT bending mode frequency renormalization curve as a function of electronic gate and bias voltages. In particular, we were able to predict features (formation of a double dip feature), at that time not yet observed, that have found successive experimental observation.[12]

In this paper we extend the approach developed in Ref. 16 to the case when the a transverse magnetic field is applied to the CNT device. The application of a field perpendicular to the current flux introduces an electronic tunneling phase which depends on the mechanical CNT displacement and therefore modifies all the terms describing the CNT-resonator dynamics. The effective force acting on the resonator is modified by a pure nonequilibrium correction term proportional to the magnetic field as well as to the electronic current.[31] This provides an interesting resonance frequency renormalization effect as a function of the magnetic field strength. We find that, increasing the magnetic field, the peculiar features (single or

double dip) observed in the bending mode resonance frequency against gate voltage curves get distorted and acquire a dip-peak structure that should be experimentally observed. In particular, this effect should be more easily detectable at bias voltages that exceed the broadening due to tunnel coupling. Our analysis concerns also the study of the device response when the CNT-resonator motion is actuated by an external antenna at fixed frequency and amplitude. In this case, the current-gate voltage characteristic exhibits specific structures corresponding to the mechanical resonances (antenna frequency equal to the bending mode frequency).

Finally, we explored the effect of the external magnetic field on the mechanical damping experienced by the CNT studying the behavior of quality factors. The magnetic field is shown to provide an additional damping mechanism for the CNT mechanical motion. Interestingly, a quadratic decrease of the quality factor Q as a function of the external magnetic field strength emerges, in quantitative agreement with the experiment performed in Ref. 1. We've also shown that, at a fixed gate, bias voltage, and temperature, if charge and current variations of the opposite sign occur, damping increases and Q is reduced. Vice versa, charge and current variations of the same sign reduce damping with a consequent increase of quality factors.

The paper is organized as follows: In Sec. II we discuss the model, In Sec. III we construct, by means of the adiabatic approximation, the stochastic Langevin equation for the dynamics of the CNT resonator including magnetic field and external antenna effects. In Sec. IV we present numerical results.

II. MODEL

We consider the system sketched in Fig. 1, which shows a single wall CNT suspended between two normal-metal leads. An external magnetic field H is applied perpendicular to the CNT oscillation plane. We also restrict the CNT mechanical degrees of freedom to the low-frequency bending mode and model it as a harmonic oscillator with frequency ω_0.

The electronic part of the CNT device is modeled as a single electronic level coupled to the leads through standard tunneling terms.[16,24] The electronic Hamiltonian is

$$\hat{\mathcal{H}}_{\rm el} = U_{\rm gate}\hat{d}^\dagger\hat{d} + \sum_{k,\alpha} V^H_{k,\alpha}(x)\hat{c}^\dagger_{k,\alpha}\hat{d} + \text{H.c.} + \sum_{k,\alpha}\varepsilon_{k,\alpha}\hat{c}^\dagger_{k,\alpha}\hat{c}_{k,\alpha}, \tag{1}$$

where the CNT's electronic level has energy $U_{\rm gate}$ with creation (annihilation) operators $\hat{d}^\dagger(\hat{d})$. The operators $\hat{c}^\dagger_{k,\alpha}(\hat{c}_{k,\alpha})$ create

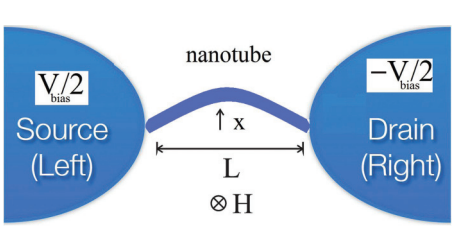

FIG. 1. (Color online) A carbon nanotube (CNT) subject to an external magnetic field H suspended between two normal-metal leads biased by a voltage $eV_{\rm bias}$.

(annihilate) electrons with momentum k and energy $\varepsilon_{k,\alpha} = E_{k,\alpha} - \mu_\alpha$ in the left ($\alpha = L$) or right ($\alpha = R$) free metallic leads. The chemical potentials in the leads μ_L and μ_R are assumed to be biased by an external voltage $eV_{\rm bias} = \mu_L - \mu_R$.

In the presence of a magnetic field, the phases of the tunneling amplitudes with the leads depend on the CNT displacement x,[33,34]

$$V^H_{k,L}(x) = V_{k,L}e^{-\imath px}, \quad V^H_{k,R}(x) = V_{k,R}e^{\imath px}, \tag{2}$$

where $p = \delta eHL/2\hbar$ gives the CNT momentum change induced by the Lorentz force when an electron tunnels from the CNT to a lead, and $\delta \simeq 1$ is a numerical factor determined by the spacial profile of the fundamental mode.[35] Above, e is the modulus of the electron charge, $\hbar$ is the Plank constant, and L is the CNT length. Slow time varying tunneling amplitudes $V_k(t)$ are also relevant in the case of adiabatic quantum pumping through quantum dots.[25,36] Furthermore, when the external magnetic-field values are sufficiently small, such as the Zeeman splitting is negligible compared to broadening due to tunnel coupling, we can neglect the effect of the electronic spin degrees of freedom.

For the sake of simplicity, we will suppose symmetric coupling $V_{k,L} = V_{k,R}$ and a flat density of states for the leads $\rho_{k,\alpha} \mapsto \rho_\alpha$, considered as thermostats at finite temperature T, within the wide-band approximation ($V_{k,\alpha} \mapsto V_\alpha$, $\alpha = L, R$).[21,37] Definitely, the total tunneling rate is $\hbar\Gamma = \sum_{\alpha=L,R}\hbar\Gamma_\alpha$, with $\Gamma_\alpha = 2\pi\rho_\alpha|V_{k,\alpha}|^2/\hbar$.

The Hamiltonian of the mechanical degree of freedom is given by

$$\hat{H}_{\rm osc} = \frac{\hat{p}^2}{2m} + \frac{1}{2}m\omega_0^2\hat{x}^2, \tag{3}$$

characterized by the frequency ω_0 and the effective mass m ($k = m\omega_0^2$). The charge-displacement interaction is provided by[37,38]

$$\hat{H}_{\rm int} = \lambda\hat{x}\hat{n}, \tag{4}$$

where λ is the charge-displacement coupling strength and $\hat{n} = \hat{d}^\dagger d$ represents the electronic charge-density on the CNT.[39] Definitely, the overall Hamiltonian is

$$\hat{\mathcal{H}} = \hat{\mathcal{H}}_{\rm el} + \hat{H}_{\rm osc} + \hat{H}_{\rm int}. \tag{5}$$

For the experiment discussed in Ref. 1, one has a strong separation between vibrational ($\omega_0 \simeq 500$ MHz $\simeq 2$ μeV) and electronic time scales ($\Gamma \simeq 50$ Ghz) so that we can solve our model in the adiabatic limit, $\omega_0/\Gamma \ll 1$. The experimental values of bias voltages and temperatures allow also a semiclassical treatment of the oscillator dynamics.[24,29,40] In this paper, we will measure lengths in units of $x_0 = r$, where r is a small fraction of CNT radius ($r = 60$ pm) appropriate to resolve the CNT bending dynamics at relatively small temperatures ($T \simeq 25$ mK). For the sake of simplicity, we will indicate dimensionless displacement variable with x. Energies are measured in units of $\hbar\Gamma = 200$ μeV, and times in units of $t_0 = 1/\omega_0$. In terms of these units, the dimensionless spring constant is $k/m\omega_0^2 \simeq 1$, since, following Ref. 1, the effective mass of the nanotube is $m = 1.3 \times 10^{-21}$ kg. Definitely, the adiabatic ratio is $\omega_0/\Gamma = 0.01$, while the dimensionless temperature $k_BT = 0.01$. Magnetic fields are measured in terms of the quantity $B = \frac{H}{H_0}$ where our magnetic

field unit is $H_0 = 2\hbar/eLr \simeq 16.6T$, since the CNT length is $L \simeq 700$ nm. Throughout this paper, we keep fixed the dimensionless charge-displacement coupling strength to $\lambda = 0.1$ (our force unit is $\hbar\Gamma/r$), corresponding to an estimate $E_p = \lambda^2/2k \simeq 1\mu eV$, implying a moderate coupling between the electronic and vibrational degrees of freedom ($E_p/\hbar\omega_0 = 0.5$). Summarizing, the regime of the relevant parameters is $\hbar\omega_0 \simeq E_p \simeq k_B T \ll eV_{\rm bias}^{\rm eff} \leqslant \hbar\Gamma$.

In the next section, we show how adiabatic approximation works on the coupled electron-oscillator problem in the presence of a transverse magnetic field.

III. ADIABATIC APPROXIMATION

As analyzed in the previous section, we work in the physical regime where the vibrational motion of the CNT resonator is "slow" with respect to all electronic energy scales and can be considered "classical": $\omega_0 \ll \Gamma$. This regime of the parameters leads to the adiabatic approximation for the electronic problem. In contrast to previous works that treated the adiabatic approximation in the absence of a magnetic field,[24–26] we here investigate the effect of a transverse magnetic field on the electronic problem described by the Hamiltonian Eq. (5). We remark that the adiabatic approximation has been used successfully for the study of spectral and transport properties of organic semiconductors.[41–43] In Appendix A, we have discussed in detail how the adiabatic approximation for the electronic problem works in the presence of a transverse magnetic field. In next subsection, we show that, even in the presence of a transverse magnetic field, the dynamics of the CNT resonator can be accurately described by a stochastic Langevin equation. Moreover we discuss the spatial dependence of the coefficients obtained in the adiabatic expansion of the electronic charge density and current.

A. Langevin equation for the oscillator

In the absence of a magnetic field, the effect of the electronic bath and the charge-displacement coupling on the oscillator dynamics gives rise to a stochastic Langevin equation with a position dependent dissipation term and white noise force.[24] As in Ref. 16, even in the present case the equation for the oscillator dynamics can be written as follows:

$$\begin{aligned} m\ddot{x} + A(x)\dot{x} &= F_{(0)}(x) + \sqrt{D(x)}\xi(t) + A_{\rm ext}\cos(\omega_{\rm ext}t), \\ \langle\xi(t)\rangle &= 0, \quad \langle\xi(t)\xi(t')\rangle = \delta(t-t'), \end{aligned} \tag{6}$$

where $\xi(t)$ is a standard white-noise term. We have included in our schematization the effect of an external antenna exciting the motion of the CNT, where $A_{\rm ext}$, $\omega_{\rm ext}$ represent the antenna amplitude and frequency, respectively. In this section, we describe how all the terms appearing in the above equation modify in the presence of an external transverse magnetic field.

The total force acting on the CNT resonator is

$$F = -kx - \lambda\langle\hat{n}\rangle(x,v) + \tilde{H}\langle\hat{I}\rangle(x,v). \tag{7}$$

The linear elastic force exerted on the oscillator is modified by two relevant *nonlinear* correction terms: the former is proportional to the electronic charge density on the CNT level Eq. (A7), while the latter is proportional to the electronic current Eq. (A17). The first term, due to the charge-displacement interaction on the CNT resonator and proportional to λ was already discussed in Refs. 2 and 16. Far from equilibrium and in the presence of a magnetic field, a magnetomotive coupling between the CNT-resonator displacement and the electronic flow comes into play. Actually, the transverse magnetic field introduces a phase in the electronic tunneling that is proportional to the CNT displacement as well as on the field strength. This originates a Lorentz-like additive correction, linear in the magnetic field strength and in the electronic current, to the average force acting on the resonator [last term in Eq. (7)].

In the limit of the adiabatic approximation, the force Eq. (7) can be decomposed in different expansion terms. It explicitly depends on the oscillator position x through $U_{\rm gate}(x) = U_{\rm gate} + \lambda x$ and velocity v. The force is

$$F(x,v) = F_{(0)}(x) + F_{(1)}(x,v), \tag{8}$$

where

$$F_{(0)}(x) = -kx - \lambda\langle\hat{n}\rangle_{(0)}(x) + \tilde{H}\langle\hat{I}\rangle_{(0)}(x), \tag{9}$$

and

$$\begin{aligned} F_{(1)}(x,v) &= -\lambda\langle\hat{n}\rangle_{(1)}(x,v) + \tilde{H}\langle\hat{I}\rangle_{(1)}(x,v) \\ &= -A(x)v. \end{aligned} \tag{10}$$

The total damping term $A(x)$ is given by three contributions,

$$A(x) = A^{\lambda}(x) + A^{H}(x) + A^{H\lambda}(x), \tag{11}$$

where both

$$A^{\lambda}(x) = \lambda R_{(1)}(x), \tag{12}$$

coming from the charge-displacement coupling, and

$$A^{H}(x) = -\tilde{H}U_{(2)}(x), \tag{13}$$

due to magnetic field coupling, are positive definite. The function $A^{H\lambda}(x)$ is proportional to both charge-displacement coupling strength λ and magnetic field H,

$$A^{H\lambda}(x) = \lambda R_{(2)}(x) - \tilde{H}U_{(1)}(x), \tag{14}$$

and is not positive definite. Remarkably, we have verified that the whole sum appearing in Eq. (11) is positive definite for the parameter regime discussed in this paper. This shows that, using a spinless fermionic model in the presence of normal (not ferromagnetic) electronic leads, the CNT resonator experiences no negative damping regions.

In our description, a fluctuating term has to be included to take correctly into account the effect of the bath degrees of freedom. When a magnetic field is present, the force-force fluctuations are given by three contributions (see Appendix B),

$$\begin{aligned} \langle\delta\hat{F}(t)\delta\hat{F}(t')\rangle &= \lambda^2\langle\delta\hat{n}(t)\delta\hat{n}(t')\rangle \\ &\quad - \tilde{H}\lambda[\langle\delta\hat{n}(t)\delta\hat{I}(t')\rangle + \langle\delta\hat{I}(t)\delta\hat{n}(t')\rangle] \\ &\quad + \tilde{H}^2\langle\delta\hat{I}(t)\delta\hat{I}(t')\rangle, \end{aligned} \tag{15}$$

where we get a mixed current-density fluctuation contribution $[\langle\delta\hat{n}(t)\delta\hat{I}(t')\rangle + \langle\delta\hat{I}(t)\delta\hat{n}(t')\rangle]$, and a current-current fluctuation contribution $\langle\delta I_\alpha(t)\delta I(t')\rangle$ to the noise.

In the adiabatic limit, exploiting the effect of the "fast" electronic environment on the oscillator motion, one derives

$$\langle \delta\hat{F}(t)\delta\hat{F}(t')\rangle = D(x)\delta(t-t'), \tag{16}$$

where in the presence of a magnetic field we have

$$D(x) = D^{\lambda}(x) + D^{H}(x) + D^{H,\lambda}(x), \tag{17}$$

with

$$\begin{aligned} D^{\lambda}(x) &= \lambda^2\hbar\int\frac{d\hbar\omega}{2\pi}G^{<}_{(0)}(\omega,x)G^{>}_{(0)}(\omega,x) \\ &= \lambda^2\hbar\int\frac{d\hbar\omega}{2\pi}\frac{\hbar\Gamma_L f_L(\omega)+\hbar\Gamma_R f_R(\omega)}{[(\hbar\omega-U_{\rm gate}(x)]^2+[\hbar\Gamma]^2/4)^2} \\ &\quad\times\{\hbar\Gamma_L[1-f_L(\omega)]+\hbar\Gamma_R[1-f_R(\omega)]\} \end{aligned} \tag{18}$$

and

$$\begin{aligned} D^{H\lambda}(x) &= \frac{e\tilde{H}}{2}\lambda\int\frac{d\hbar\omega}{2\pi}\left|G^{r}_{(0)}(\omega,x)\right|^2 C(\omega,x) \\ &\quad\times\left(\Sigma^{L,>}_{(0)}(\omega)\Sigma^{L,<}_{(0)}(\omega)-\Sigma^{R,<}_{(0)}(\omega)\Sigma^{R,>}_{(0)}(\omega)\right) \\ &= e\lambda\tilde{H}\int\frac{d\hbar\omega}{2\pi}\frac{\hbar\Gamma_L+\hbar\Gamma_R}{\{[\hbar\omega-U_{\rm gate}(x)]^2+[\hbar\Gamma]^2/4\}^2} \\ &\quad\times\{[\hbar\Gamma_L]^2 f_L(\omega)[1-f_L(\omega)]-[\hbar\Gamma_R]^2 f_R(\omega) \\ &\quad\times[1-f_R(\omega)]\}, \end{aligned} \tag{19}$$

where $C(\omega,x) = -2{\rm Im}G^{r}_{(0)}(\omega,x)$ is the electronic spectral function of the electronic level defined in Eq. (A9). The noise strength contribution coming from current-current fluctuations is

$$\begin{aligned} D^{H}(x) &= \frac{e^2}{\hbar}\tilde{H}^2\int\frac{d\hbar\omega}{2\pi}[f_L(\omega)-f_R(\omega)]^2 T(\omega,x) \\ &\quad\times[1-T(\omega,x)]+\{f_L(\omega)[1-f_L(\omega)] \\ &\quad+f_R(\omega)[1-f_R(\omega)]\}T(\omega,x), \end{aligned} \tag{20}$$

where $T(\omega,x) = \frac{\hbar\Gamma}{4}C(\omega,x)$. In the absence of bias voltage, one has $D(x) = 2k_BTA(x)$, that is, the fluctuation-dissipation condition is verified for each fixed position x. Moreover, it is possible to show that in the chosen units, the dimensionless damping $A(x)$ [Eq. (11)] and diffusive term $D(x)$ [Eq. (17)] result proportional to the adiabatic ratio ω_0/Γ.

It is important to point out that, when there is no intrinsic charge-displacement coupling ($\lambda = 0$), in the absence of the antenna effects and at zero bias ($V_{\rm bias} = 0$), the oscillator is still governed by a Langevin equation

$$m\ddot{x} + A^{H}(x)\dot{x} = kx + \sqrt{D^{H}(x)}\xi(t), \tag{21}$$

with a harmonic force $F_{(0)}(x) = -kx$, an intrinsic positive-definite dissipative term $A^{H}(x)$, and a diffusive term $D^{H}(x)$ proportional to the thermal current-current noise. Looking at Eqs. (13) and (20) together with Eq. (10), one can clearly see that a natural quadratic dependence of damping and diffusive strength on the magnetic field emerges. This can be explained observing that, even at zero bias voltage, the electronic tunneling events, whose phase is dependent linearly on the CNT displacements as well as on the magnetic-field strength, perturb the CNT mechanical motion with a force with zero average (due to $\langle\hat{I}\rangle = 0$, $\tilde{H}$ can be also different from zero) and square mean proportional to the magnetic field square. Definitely, even in the absence of external bias voltage $V_{\rm bias}$, the magnetic field applied perpendicular to the CNT couples to the bending mode dynamics behaving as a surrounding thermal bath at leads temperature k_BT.

We end this section pointing out that our system is conceptually different from those discussed in Refs. 34 and 30. In Ref. 34, the authors use a normal and a ferromagnetic lead and observe negative damping and consequent nanoelectromechanical self-excitations of the CNT-resonator system. In that case, a strong correlation of tunneling processes of spin up and spin down electrons is realized from and to the leads, which results in a pumping of energy in the mechanical vibrating CNT. Instead, when the CNT is described as a single spinless electronic level, electrons tunnel randomly from the leads to the CNT dot (and vice versa) and interact with the mechanical resonator through a coupling between the CNT charge density and the CNT displacement x. By virtue of this interaction, uncorrelated random tunneling events from and to the leads (assumed at equilibrium) perturb the CNT displacement x, resulting in a diffusive motion of the mechanical resonator. Indeed, in this case the positive damping or friction is induced by the retardation of the electronic degrees of freedom, which do not respond immediately to a change in x (first nonadiabatic correction).[24,29] When a transverse magnetic field is applied, electronic tunneling processes lead to random changes of the nanotube momentum, which results in a diffusive motion in its phase space. Therefore, even in the presence of a magnetic field, the effect of the electronic environment on the vibrating CNT can be described by an uncorrelated (multiplicative) white noise and positive definite friction. As we will see below, at thermodynamic equilibrium, the noise strength is directly related to the electronic current-current fluctuations across the CNT dot which are naturally positive definite and proportional to the friction term Eq. (13). Finally, we mention that in Ref. 30, it has also been verified that in the case of a double quantum dot with the oscillator coupled with the difference of population between the dots, one can have a negative friction term in some regions of configuration space of the oscillator.

B. Spatial dependence of the Langevin equation coefficients

In this section we perform a systematic study of the spatial dependence of the total force, the damping (see Fig. 3) and diffusive terms (see Fig. 4) as a function of the bias voltage as well as on the magnetic-field strength.

As concerns the total force acting on the CNT resonator, we point out that, for the magnetic field strengths investigated in this paper, the effective potential preserves its parabolic shape with a displaced minimum and renormalized curvature. For instance, when a left-to-right current flows through the device (see the sketch in Fig. 1) in the presence of a positive magnetic field (outgoing from the sketch reported in Fig. 1), the CNT-resonator effective potential minimum is displaced towards positive displacements x with respect to the minimum set by the charge-displacement interaction [see Figs. 2(a) and 2(b)]. In Fig. 2, one can observe that the minimum of the effective potential acting on the resonator depends linearly on the magnetic field strength. This comes from the linear dependence on the magnetic field of the Lorentz-like correction term to the force, Eq. (9). In particular, as shown in Fig. 2(a), in the low bias regime for the device (small

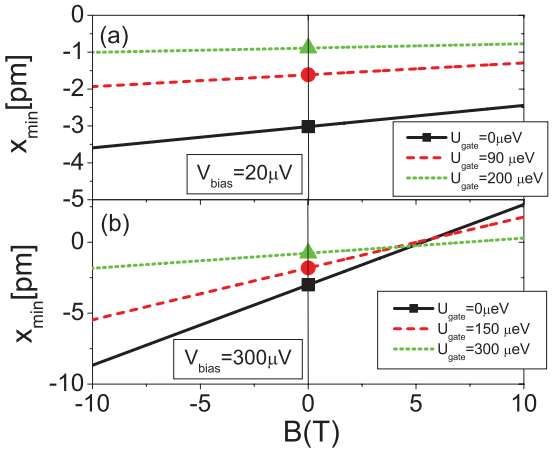

FIG. 2. (Color online) (a) Minimum of the effective potential [coming from the force Eq. (9)] affecting the CNT resonator as a function of the magnetic field at low bias $eV_{\rm bias} = 0.1\hbar\Gamma$ ($V_{\rm bias} = 20\ \mu$V in our units). Solid (black) line indicates $U_{\rm gate} = 0$, dashed (red) line $U_{\rm gate} = 0.45$ ($V_{\rm bias} = 90\ \mu$V in our units), dotted (green) line $U_{\rm gate} = 1.0$ ($V_{\rm bias} = 200\ \mu$V in our units). (b) Same as above at large bias $eV_{\rm bias} = 1.5\hbar\Gamma$ ($V_{\rm bias} = 300\ \mu$V in our units). Solid (black) line indicates $U_{\rm gate} = 0$, dashed (red) line $U_{\rm gate} = 0.75$ ($V_{\rm bias} = 150\ \mu$V in our units), dotted (green) line $U_{\rm gate} = 1.5$ ($V_{\rm bias} = 300\ \mu$V in our units).

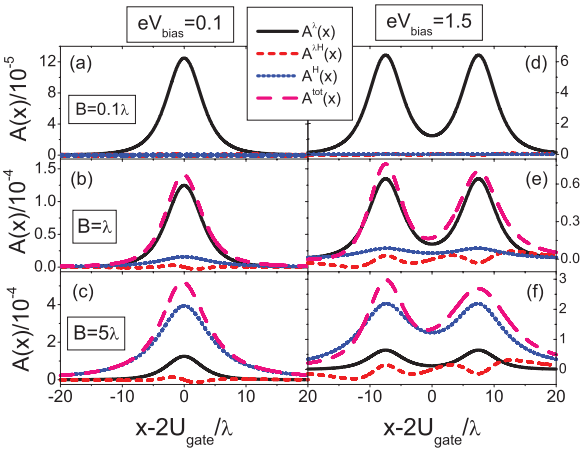

FIG. 3. (Color online) Spatial dependence of the dimensionless damping coefficient $A(x)$ at low bias (a)–(c) and at large bias voltage applied (d)–(f). See main text for discussion.

compared to the broadening of the CNT level), the larger is the gate voltage, the smaller is the displacement of the potential minimum as a function of the external magnetic field with respect to the shift produced by the charge-displacement interaction [whose position is indicated by a (black) square for $U_{\rm gate} = 0$, a (red) circle for $U_{\rm gate} = 0.45$ ($V_{\rm bias} = 90\ \mu$V in our units), and a (green) triangle $U_{\rm gate} = 1.0$ ($V_{\rm bias} = 200\ \mu$V in our units)]. This can be explained observing that in the low conducting regime of the device the resonator is less effectively coupled with the electronic subsystem. In the large bias regime [Fig. 2(b)], a smaller magnetic field is sufficient to displace the potential minimum of the same quantity produced by the sole charge-displacement interaction on the CNT. Again, the larger the gate voltage, the smaller the displacement of the potential minimum as a function of the external magnetic field with respect to the shift produced by the charge-displacement interaction.

The renormalization of the effective potential curvature, that is, of the resonance frequency of the resonator, will be discussed in subsection A of the next section.

In this section, we limit ourselves to discuss the damping term $A(x)$, since for the diffusive term $D(x)$, unless explicitly stated, a similar analysis can be done. As shown above [see Eq. (11)], we can distinguish between three contributions to the friction affected by the oscillator: a *pure* charge-displacement contribution $A^{\lambda}(x)$, depicted in Fig. 3 with a solid (black) line, already discussed in Refs. 24 and 30; a damping contribution due to current-current fluctuations $A^{H}(x)$, depicted in Fig. 3 with a dotted (blue) line; a mixed damping term due to current-density fluctuations (not positive definite), indicated by $A^{\lambda H}(x)$ and depicted in Fig. 3 with a short-dashed (red) line. The total damping $A(x)$ is reported with a dashed (pink) line. As one can observe in panel (a), at low bias voltage, when the external magnetic field strength is smaller than charge-displacement coupling λ, the damping contributions coming from the current-current $A^{H}(x)$ and current-density $A^{\lambda H}(x)$ fluctuations are negligible with respect to that generated by the *pure* charge-displacement contribution $A^{\lambda}(x)$. In panel (a), $A^{\lambda}(x)$ and $A^{H}(x)$ have a single peak structure centered at $x - 2U_{\rm gate}/\lambda \simeq 0$, while $A^{\lambda H}(x)$ is an odd symmetric function with respect to this point. We point out that these peculiar structures are visible only at larger values of magnetic field [Figs. 3(b) and 3(c)]. The total damping affecting the resonator is peaked at configurations where large density variations take place $|x - 2U_{\rm gate}/\lambda| < \hbar\Gamma/\lambda$. Indeed, the density of the CNT level goes from a region $x - 2U_{\rm gate}/\lambda < -\hbar\Gamma/\lambda$ corresponding to almost completely filled states ($\langle n\rangle \sim 1$) to a region $x - 2U_{\rm gate}/\lambda > \hbar\Gamma/\lambda$ corresponding to completely empty states ($\langle\hat{n}\rangle \sim 0$). Definitely, the CNT level experiences a unit charge variation across the $|x - 2U_{\rm gate}/\lambda| < \hbar\Gamma/\lambda$ region.[12,16]

At large bias voltages applied [panel (b)], $A^{\lambda}(x)$ has two peaks centered at $x - 2U_{\rm gate}/\lambda \simeq eV_{\rm bias}/2\lambda$ and $x - 2U_{\rm gate}/\lambda \simeq -eV_{\rm bias}/2\lambda$, respectively. $A^{H}(x)$ shows the same behavior, while $A^{\lambda H}(x)$ is an odd symmetric function with respect to these two points. As in panel (a), $A^{H}(x)$ and $A^{\lambda H}(x)$ are negligible with respect to $A^{\lambda}(x)$. The total damping affecting the resonator is peaked at configurations where the CNT level experiences a half unit charge variation across the $|x - 2U_{\rm gate}/\lambda \pm eV_{\rm bias}/2\lambda| < \hbar\Gamma/\lambda$ regions.[12,16]

When the external magnetic field is turned on, an enhanced damping as well as as noise strength emerges with a quadratic dependence on the magnetic field intensity, Eqs. (11)–(17). In Figs. 3(b) and 3(c), one can observe that, as the dimensionless ratio B/λ is equal to 1, the total damping affecting the resonator is only slightly perturbed by the application of the magnetic field. At low bias, $A(x)$ preserves its single peak structure with an enhanced strength [dashed (pink) curve in Fig. 3(b)]. At large bias, the strength of the two peaks becomes asymmetric, with an enhanced damping of the peak at $x - 2U_{\rm gate}/\lambda \simeq -eV_{\rm bias}/2$. This effect can be explained as follows: When a magnetic field is applied to the device, the resonator starts to feel even the variations of the electronic

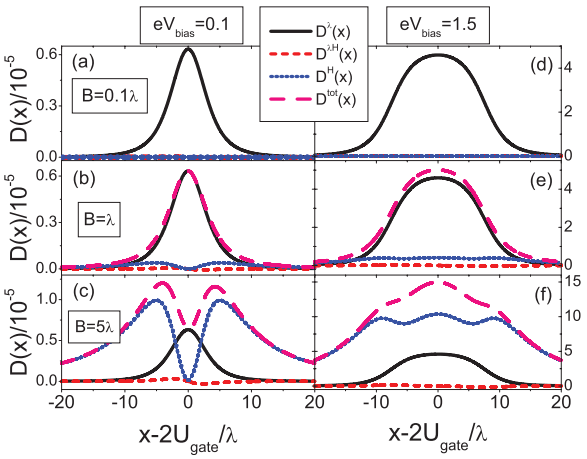

FIG. 4. (Color online) Spatial dependence of the dimensionless diffusive coefficient $D(x)$ at large bias voltage applied (a)–(c). See main text for discussion.

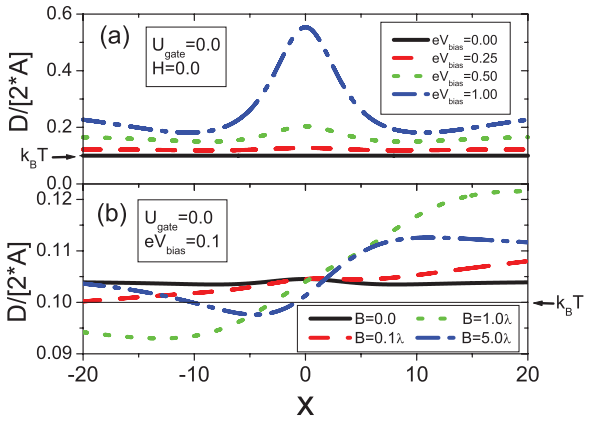

FIG. 5. (Color online) (a) Spatial dependence of the ratio $D(x)/2A(x)$ at fixed gate voltage $U_{\rm gate} = 0.0$ and zero magnetic field $B = 0.0$, electron-oscillator coupling $\lambda = 0.1$, temperature $k_BT = 0.1$, for different values of the bias voltage: solid (black) line $eV_{\rm bias} = 0.0$, dashed (red) line $eV_{\rm bias} = 0.25$, dotted (green) line $eV_{\rm bias} = 0.5$, and dashed-dotted (blue) line $eV_{\rm bias} = 1.0$. (b) Same as (a) at fixed gate voltage $U_{\rm gate} = 0.0$ and bias voltage $eV_{\rm bias} = 0.1$, for different values of the magnetic field strength: solid (black) line $B = 0.0$, dashed (red) line $B = 0.1\lambda$, dotted (green) line $B = 1.0\lambda$, and dashed-dotted (blue) line $B = 5.0\lambda$.

current flowing through the CNT as a function of the gate voltage [see Eq. (9)]. These current variations are positive for $x - 2U_{\rm gate}/\lambda < 0$ and negative otherwise. At $x - 2U_{\rm gate}/\lambda \simeq -eV_{\rm bias}/2$, large negative variations of the electronic density and positive variations of the electronic current cooperate giving an enhanced damping.

We intend now to study the regime realized when the external magnetic field strength is larger than charge-displacement coupling strength λ. In this case, the contribution to the damping coming from the current-current fluctuations $A^H(x)$ are dominant with respect to those corresponding to charge-displacement $A^\lambda(x)$ and current-density $A^{\lambda H}(x)$ fluctuations. In the low bias regime, the total damping term preserves its single peak structure which, due to the intrinsic asymmetry of the current-density term $A^{\lambda H}(x)$, is slightly distorted. For the same reason, in the large bias regime, the double dip structure of the total damping term is preserved with an enhanced asymmetry. In the large magnetic field regime, it is important to point out the particular spatial dependence of the noise strength $D(x)$ [Figs. 4(c)–4(f)]. Here, the noise contribution due to the current-current fluctuations [$D^H(x)$] emerges with the characteristic double peak structure even at low bias regime [dotted (blue) curve in Fig. 4(c)]. Comparing the dashed (pink) curves in panel (c) of Figs. 3 and 4, one can observe that, even at low bias voltage, the application of a large magnetic field drives the CNT resonator far out of equilibrium, breaking the validity of the Einstein relation $D(x) = 2k_BT_{\rm eff}A(x)$ with an effective temperature. Far from equilibrium, this relation is strictly valid only at very low bias voltages.[24,40] In order to clarify this point, in Fig. 5(b) we have plotted the ratio $D(x)/2A(x)$ as a function of the CNT displacement x, for small bias voltage $eV_{\rm bias} = 0.1$ keeping fixed $\lambda = 0.1$ and gate voltage $U_{\rm gate} = 0.0$. As the reader can observe, the solid (black) line (representing the result for zero magnetic field) can be safely considered constant and lies above the thin straight line representing the equilibrium temperature $k_BT = 0.1$. For small bias voltages ($eV_{\rm bias} < 0.4\hbar\Gamma$) the nonequilibrium electronic bath affects the CNT vibrating dynamics as a standard thermal bath at an effective temperature that in this case is $k_BT_{\rm eff} \simeq 0.104$. In Fig. 5(a), we have shown how the ratio $D(x)/2A(x)$ against displacement x starts to differ more and more from the straight equilibrium line $k_BT = 0.1$ as the bias voltage is increased.

When the magnetic field is turned on, the $D(x)/2A(x)$ curves get asymmetric as a function of displacement deviating more and more from a straight line as the magnetic field strength is increased. One can note that, even for the case with $B = 5\lambda$, the dotted (green) line curve deviates from the equilibrium temperature line by 10% at most for negative displacements and by 20% at most for positive displacements. The origin of this asymmetrization effect can be ascribed the to so-called mixed terms, $A^{\lambda H}(x)$ and $D^{\lambda H}(x)$ which are not positive definite. They are negative for $x - 2U_{\rm gate}/\lambda < 0$, where one has electronic density and electronic current variations of opposite sign (this region is characterized by an enhanced damping), and positive otherwise.

In the next section, we study numerical results of our model concerning mechanical properties of CNT resonator (resonance frequency and quality factor) as well as the electronic observables inherent to the transport problem (I-V characteristic).

IV. MECHANICAL AND ELECTRONIC CHARACTERISTICS OF THE DEVICE

Given the assumption about the separation between the slow vibrational and fast electronic (tunneling) time scales, the problem of evaluating a generic observable (electronic or not) of the system reduces to the evaluation of that quantity for a fixed position x and velocity v of the oscillator, with the consequent averaging over the stationary probability distribution $P(x,v)$. From the solution of the Langevin equation (6), one can determine the distribution $P(x,v)$ which allows us to calculate all the electronic observables O:

$$\langle O\rangle = \int dxdvP(x,v)O(x,v). \qquad (22)$$

We analyze in the next section the effects of the magnetic field on the mechanical as well as electronic properties of the device.

A. Resonance frequency renormalization and current-voltage curves

In this section, we address the magnetic field effects on the renormalization of the CNT-resonator resonance frequencies and its back-action effects on the current voltages curves of the device. In order to study the CNT resonance frequency renormalization as a function of the gate voltage, we have compared results coming from two ways of evaluation of the resonance frequencies. In the first method, referred to as *static*, we evaluate the position of the minima of the static potential arising from the generalized force acting on the resonator [Eq. (9)]. In the second method, referred to as *dynamic + antenna*, we have analyzed, at every fixed value of the gate voltage, all the traces of electronic current as a function of the antenna frequency reporting with a red thin (blue thick) line the resonance frequency values with positive (negative) current change $\Delta I = I - I_0$ with respect to background value I_0 obtained in the absence of the antenna [see Figs. 6(b)–6(d)].

In Fig. 6, we report the resonance frequencies of the CNT resonator as a function of the gate voltage comparing the two methods outlined above. We address the low bias regime in panels (a) and (b), while the large bias regime is investigated in panels (c) and (d). In Fig. 6(a), different curves, from thicker to thinner, refer to increasing magnetic field applied to the device $B = 0.0$–1.5–3.0. The same description was done in panel (c),

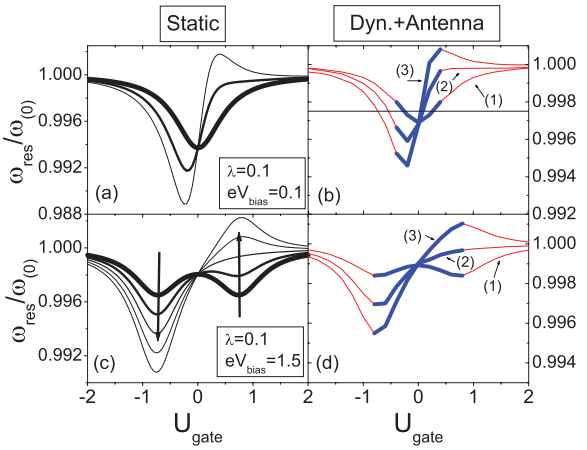

FIG. 6. (Color online) (a) Resonator frequency against effective gate voltage calculated as minimum of the effective potential in the static approximation at small bias $eV_{\rm bias} = 0.1\hbar\Gamma$ for different magnetic field values: solid thick line $B = 0.0$, solid normal-thickness line $B = 1.5$, solid thin line $B = 3.0$. (c) Same as (a) at large bias $eV_{\rm bias} = 1.5\hbar\Gamma$ for different magnetic field values: from thicker to thinner line $B = 0.0$–0.1–0.2–0.3–0.4. (b)–(d) Resonator frequency calculated using an external antenna (with $A_{\rm ext} = 10^{-3}$) at mechanical resonance against effective gate voltage for same parameters of (a)–(c), respectively. Dashed (red online) and solid (blue online) portions of each curve indicate resonance frequency values with positive and negative current change ΔI, respectively. In (d), only curves referring to magnetic field strengths $B = 0.0$–0.2–0.4 are reported.

where different curves refer to increasing magnetic field in the range $B = 0.0$–0.2–0.4. The thicker (black) lines in panels (a) and (c), corresponding to the absence of magnetic field, reproduce qualitatively all results experimentally observed in Ref. 12: when bias voltages are smaller than the broadening due to tunnel coupling [panel (a)], the resonance frequency shows a single dip as a function of gate voltage. At bias voltages that exceed the broadening due to tunnel coupling [panel (c)], the resonance frequency shows a double dip structure. Actually, in this regime, the onset of a double dip structure was already predicted by us in Ref. 16. It is important to point out that the resonance frequency renormalization curves obtained in the presence of the external antenna [Figs. 6(b)–6(d)] have the same qualitative behavior (as a function of the gate) of those obtained in the static approach. In the presence of an external antenna with a finite amplitude, renormalization effects in the resonance frequencies are less pronounced due to nonlinear softening.[2,16]

As already analyzed in Refs. 2 and 16, when the device is in a low current-carrying state, a peak in the current-frequency curve signals the mechanical resonance [whose position is indicated by thin (red) lines in Figs. 6(b)–6(d)], while in a high current-carrying state, a dip in the current-frequency curves is observed [whose position is indicated by thick (blue) lines in Figs. 6(b)–6(d)]. In the presence of a transverse magnetic field, the different character of low and high conducting states, signaled by a peak or a dip in current-frequency curves, is preserved [curves (2) and (3) in Figs. 6(b)–6(d)].

The peculiar features of CNT-resonator frequency renormalization as a function of the gate can be explained as follows. In the absence of magnetic field, the resonator frequency renormalization is maximum at electronic configurations where the the CNT level experiences the largest charge-density variations against the gate voltage,

$$k_{\rm eff} = k + \lambda^2 \frac{\partial \langle \hat{n} \rangle}{\partial U_{\rm gate}}\bigg|_{x=x_{\rm min}}. \tag{23}$$

Actually, at low bias voltages, a unit charge density variation across the region where the small conduction window is placed $|U_{\rm gate}| < \hbar\Gamma$ [solid (black) thick line in Fig. 6(a)] occurs. At large bias voltages, the CNT frequency renormalization is larger at electronic configurations where the CNT level experiences a half unit charge variation, that is, at $|U_{\rm gate} - eV_{\rm bias}/2| < \hbar\Gamma$ and at $|U_{\rm gate} + eV_{\rm bias}/2| < \hbar\Gamma$.

When the transverse magnetic field is turned on, the above scenario modifies as follows. The resonator frequency renormalization is larger at electronic configurations where the CNT level experiences the largest charge density *and* current variations against the gate voltage,

$$k_{\rm eff} = k + \lambda^2 \frac{\partial \langle \hat{n} \rangle}{\partial U_{\rm gate}}\bigg|_{x=x_{\rm min}} - \lambda \tilde{H} \frac{\partial \langle \hat{I} \rangle}{\partial U_{\rm gate}}\bigg|_{x=x_{\rm min}}. \tag{24}$$

At low bias voltage, the single dip feature in the CNT-resonator resonance frequency gets distorted [solid normal-thickness line in Fig. 6(a)] and acquires, in the limit of large magnetic field [solid thin line in Fig. 6(a)], a dip-peak structure that could be experimentally observed. Actually, the peak observed at $U_{\rm gate} \simeq 0.3$ corresponds to a hardening of the CNT-resonator resonance frequency. This effect can be explained as follows:

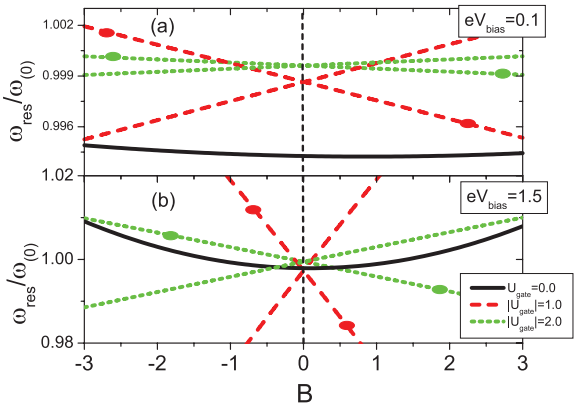

FIG. 7. (Color online) (a) Resonator frequency against magnetic field strength calculated as minimum of the effective potential in the static approximation at small bias $eV_{\rm bias} = 0.1\hbar\Gamma$ for different gate voltage values: solid (black) line $U_{\rm gate} = 0.0$, dashed (red) line $U_{\rm gate} = 1.0$, dashed (red) line marked with a full circle $U_{\rm gate} = -1.0$, dotted (green) line $U_{\rm gate} = 2.0$, dotted (green) line marked with a full circle $U_{\rm gate} = -2.0$. (b) Same as (a) at large bias $eV_{\rm bias} = 1.5\hbar\Gamma$ for same gate voltage values of (a).

when a magnetic field is applied to the device, the resonator starts to feel even the variations of the electronic current flowing through the CNT as a function of the gate voltage [see Eq. (24)]. These current variations are positive for $U_{\rm gate} < 0$ and negative otherwise. At $U_{\rm gate} \simeq 0.3$, the positive (due to the positive sign of the magnetic field) variations of the electronic current overcome the negative variation of the electronic density giving a hardening in the CNT resonance frequency. At $U_{\rm gate} \simeq -0.25$, one has negative variations of both density and current, obtaining a more pronounced softening in the resonance frequency. The effect outlined above is more pronounced in the large bias regime [see Fig. 6(c)]. Here, the magnetic field gives an enhanced softening dip at $U_{\rm gate} \simeq -eV_{\rm bias}/2$ and a hardening peak at $U_{\rm gate} \simeq eV_{\rm bias}/2$, where positive variations of the electronic current cooperate with negative variation of the electronic density. In both low and high bias regime, the hardening effect outlined above could be experimentally observed.

We can now complete the analysis of renormalization frequency effects by studying their dependence on the magnetic field strength at fixed gate voltage. In Fig. 7(a), we show the resonance frequency curves in the low bias voltage $eV_{\rm bias} = 0.1$ regime obtained in the static approximation against magnetic field strength for different values of the gate voltages. Both in the low [panel (a)] and high voltage regimes [panel (b)], one can observe that only when the device is in high conducting state [solid (black) curve for $U_{\rm gate} = 0.0$] the resonance frequency curves show a quadratic dependence on the magnetic field strength. We have verified numerically that this quadratic behavior is present only for a very narrow interval of gate voltage values $|U_{\rm gate}| < 0.2\hbar\Gamma$. When the device is pushed to low conducting states [dashed $U_{\rm gate} = 1$ (red) and dotted $U_{\rm gate} = 2$ (green) lines in Fig. 7(a)] the resonance frequency curves change character showing a linear dependence on the magnetic field strength (in the range of magnetic field values experimentally investigated, $|B| < 1$). In particular, for positive gate voltages one has an increase of the frequency going towards a hardening effect. For negative gate voltages (curves are marked with full circles), frequency decreases obtaining an enhanced softening. In the high voltage bias regime, the same behavior can be observed, but with a larger renormalization of frequencies in the magnetic field strength interval. This difference is easily understood observing that in this case the correction to the CNT frequency is proportional to the magnetic field strength [see Eq. (24)]. The effect outlined above can be explained as follows. When the device is in a high conducting state ($|U_{\rm gate}| < 0.2\hbar\Gamma$), the CNT dynamics is effectively strongly coupled to the electronic current flow. In this case, the equilibrium displacement $x_{\rm min}$ (discussed in the previous section in Fig. 2) of the CNT is more easily tunable as a function of the magnetic field strength giving an effective quadratic dependence of the last term of Eq. (24) on it (actually $\frac{\partial\langle\hat{I}\rangle}{\partial U_{\rm gate}}|_{x=x_{\rm min}}$ gets a linear dependence on H). When the device is in a low conducting state, the CNT equilibrium displacement $x_{\rm min}$ depends only slightly on the magnetic field strength, therefore the coefficient $\frac{\partial\langle\hat{I}\rangle}{\partial U_{\rm gate}}|_{x=x_{\rm min}}$ in Eq. (24) is practically constant in all the range of physically investigated magnetic field values.

Coming back to Fig. 7(a), one can see that in the low bias regime and for $U_{\rm gate} = 0.0$ frequency decreases for positive magnetic field strength and then reaches a minimum for $B \simeq 0.8$. On the contrary, in the high bias voltage regime [panel (b)], the frequency has a minimum for a smaller value of the magnetic field $B \simeq 0.05$. We have verified numerically that for $U_{\rm gate} = 0$ the minimum position of the frequency-magnetic feld curve is proportional to the magnetic field strength for which one has a zero displacement for the CNT, $B_{\rm min} \propto B(x = 0)/2$. These two quantities go to zero increasing the bias voltage. This behavior can also be expected looking at Fig. 2(b), where one can see that, if the bias voltage is sufficiently large, a smaller and smaller positive magnetic field is required to put the CNT displacement to zero.

The peculiar renormalization frequency effects discussed above have a nontrivial back-action effects on the electronic density and current-gate voltage characteristic of the device. In Fig. 8, we study the electronic CNT level density and current as a function of the gate voltage in the presence of an external antenna at fixed amplitude and frequency $\omega_{\rm ext} = 0.9975$ [corresponding to the horizontal line in Fig. 6(b)] in the low bias regime of the device.[44] When the external antenna frequency becomes equal to the proper frequency of the resonator, we observe a dip structure in both density and current at a gate voltage corresponding to high conducting states of the device [solid (black) line in Figs. 8(a) and 8(b)]. This feature, that could be experimentally observed, is considered as a "dip" with respect to corresponding curves in the absence of antenna or with an antenna frequency far from the range of the proper frequencies of the CNT resonator (not shown in Fig. 8).

When a transverse magnetic field is applied to the device, the CNT frequency renormalization profile as a function of the gate voltage changes (see Fig. 6). Therefore, the mechanical resonance condition between the external antenna frequency and the proper frequency of the resonator occurs at different electronic gate voltages. For sufficiently large magnetic fields, the resonance can occur in correspondence of a low conducting

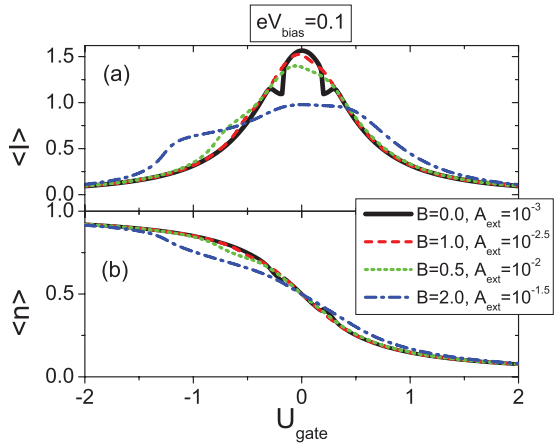

FIG. 8. (Color online) (a) Average electronic current flowing through the CNT level at low bias ($eV_{\rm bias} = 0.1$) as function of the gate voltage for different values of the magnetic field and in the presence of a external antenna applied to the device at fixed frequency $\omega_{\rm ext} = 0.9975$ and amplitude: solid (black) line $A_{\rm ext} = 10^{-3}$, dashed (red) line $B = 1.0A_{\rm ext} = 10^{-2.5}$, dotted (green) line $B = 1.5A_{\rm ext} = 10^{-2.0}$, dashed-dotted (blue) line $B = 1.0A_{\rm ext} = 10^{-2.5}$. (b) Average electronic density on the CNT level for the same parameter values as in (a). See the main text for detailed discussion.

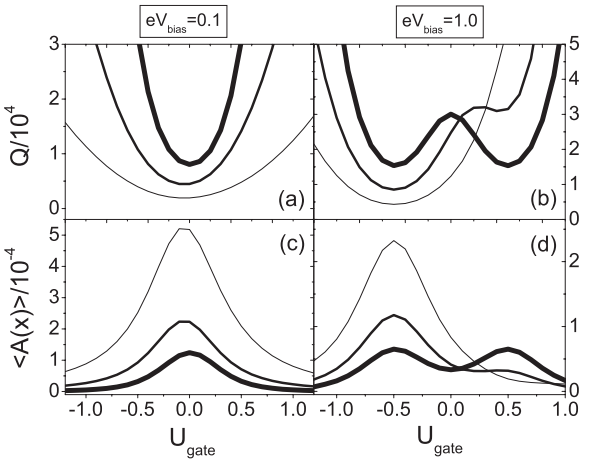

FIG. 9. Device quality factor as a function the gate voltage $U_{\rm gate}$ for different magnetic field strengths at low (a) and large (b) bias voltage. (c), (d) Same as above for the average total damping $\langle A(x)\rangle$ of the system. (a)–(c) Solid thick line $B = 0.0$, solid normal-thickness line $B = 1.5$, and solid thin line $B = 3.0$. (b)–(d) Solid thick line $B = 0.0$, solid normal-thickness line $B = 0.2$, and solid thin line $B = 0.4$.

state of the device. As one can observe in Figs. 8(a) and 8(b), a dip structure in the electronic density at a more negative gate voltage and corresponding current peak [dotted (green) and dashed-dotted (blue) lines in Figs. 8(a) and 8(b)] is visible. Actually, the above structures are broadened due the reduction of the quality factor as a function of the magnetic field. In the limit of very large magnetic fields, if we keep fixed the amplitude of the external antenna, the fine structures outlined above are completely washed out due to the decrease of the device quality factors.

B. Device quality factors

One of the main findings of Ref. 1 is the observation of a quadratic dependence of the device quality factor Q on external magnetic field strength. Within our model, as also stressed in the previous sections, such a quadratic dependence on B emerges naturally. In order to include back-action effects of the out-of-equilibrium electronic bath on the resonator, we have calculated the average device quality factor as

$$Q = \int_{-\infty}^{\infty} dx \frac{1}{A(x)} P(x), \tag{25}$$

where $A(x)$ is the total damping at a particular resonator displacement x and $P(x)$ is the reduced displacement distribution probability of the CNT resonator. We have verified that this particular way of extracting quality factors is completely equivalent to measure the width half high in the current-frequency curves obtained in the linear response to an external antenna exciting the nanotube motion.[16]

Motivated by the experiment performed in Ref. 1 and by recent experimental study on a similar CNT device,[12] we here performed a systematic study of the quality calculated from our model as a function of the bias, gate voltage, as well as on the magnetic field. In Figs. 9(a) and 9(b), we investigate the device quality factor Q as a function of gate voltage in the low and large bias voltage regime, respectively. In the absence of a transverse magnetic field, we reproduce the qualitative behavior obtained in the experiment of Ref. 12. When bias voltages are smaller than the broadening due to tunnel coupling, the quality factor shows a single dip feature [solid (black) thick line in Fig. 9(a)]. At bias voltages that exceed (or are equal to) the broadening due to tunnel coupling, the quality factor shows a double dip structure [solid (black) thick line in Fig. 9(b)]. This behavior, already addressed in Refs. 12 and 16, can be easily explained looking at the average charge and dissipation of the CNT resonator. As also discussed referring to total damping affecting the CNT resonator in Sec. III B, at low bias voltage and in the absence of magnetic field, the total average damping affecting the resonator is peaked at electronic configurations where the CNT level experiences a unit charge variation across the region where the small conduction window is placed $|U_{\rm gate}| < \hbar\Gamma$ [solid (black) thick line in Fig. 9(c)]. At large bias voltages, the conduction window, whose extension is proportional to $eV_{\rm bias}$, becomes larger than the broadening of the CNT level, so that the total average damping affecting the resonator is peaked at electronic configurations where the CNT level experiences half unit charge variations, that is, at $|U_{\rm gate} - eV_{\rm bias}/2| < \hbar\Gamma$ and $|U_{\rm gate} + eV_{\rm bias}/2| < \hbar\Gamma$. When the transverse magnetic field is turned on, the above scenario modifies as follows. At low bias voltages, the total damping affected by the CNT resonator increases quadratically with the field at every point in the configuration space of the oscillator. Moreover, the CNT-resonator distribution probabilities $P(x)$ depend slightly on the magnetic field as well as on the gate voltages and are actually centered at configurations close to the harmonic potential minimum $x \simeq 0$ in the absence of charge-displacement interaction λ. The overall result is an enhanced average total damping as one increases the magnetic field [solid normal-thickness ($B = 1.5$) and thin ($B = 3.0$) (black) lines in Fig. 9(c)] and a corresponding decrease of

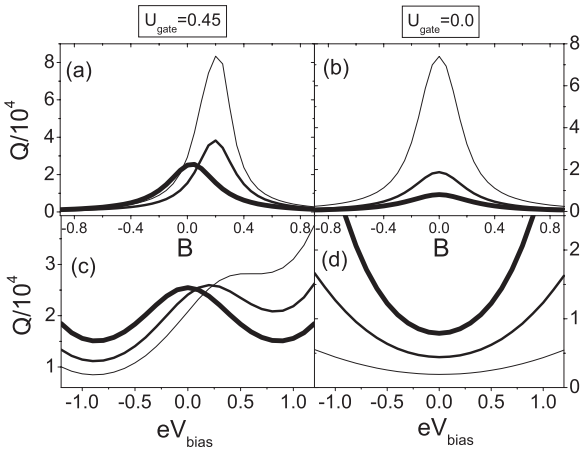

FIG. 10. Device quality factor as a function the magnetic field strength B for different bias voltages (solid thick line $eV_{\rm bias} = 0.1$, solid normal-thickness line $eV_{\rm bias} = 0.75$, and solid thin line $eV_{\rm bias} = 1.5$) at low (a) and high (b) conducting states. (c),(d) Device quality factor as a function of the bias voltage $eV_{\rm bias}$ for different magnetic field strengths at low (c) and high (d) conducting states. (c) Solid thick line $B = 0.0$, solid normal-thickness line $B = 0.05$, and solid thin line $B = 0.1$. (d) Solid thick line $B = 0.0$, solid normal-thickness line $B = 0.25$, and solid thin line $B = 0.5$.

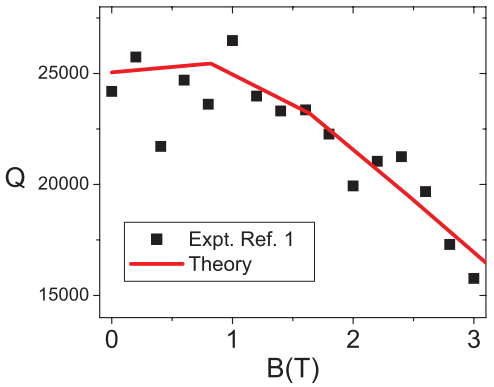

FIG. 11. (Color online) Device quality factor as a function the magnetic field strength. Squares represent experimental values obtained in Ref. 1 at $T = 25$ mK, $V_{\rm bias} = 0.3$ mV, and distance from the current peak $U_{\rm gate} = -90$ mV. Solid (red) line is calculated Q at $k_BT = 0.01$, $eV_{\rm bias} = 0.1$, and $U_{\rm gate} = 0.45$.

the quality factor in all the gate voltage range investigated [solid normal-thickness ($B = 1.5$) and thin ($B = 3.0$) (black) lines in Fig. 9(a)]. At large bias voltage, the $P(x)$ still depends only slightly on the magnetic field but is very spread on the configuration space. Therefore, the average in Eq. (25) reproduces the spatial dependence structure of the total damping coefficient reciprocal $1/A(x)$. The double peak structure of the average total damping term [solid thick (black) line in Fig. 9(d)] is canceled by the magnetic field, giving a single peak at $U_{\rm gate} = eV_{\rm bias}/2$ where a cooperation between negative charge density and positive current variations take place [solid normal-thickness ($B = 0.2$) and thin ($B = 0.4$) (black) lines in Fig. 9(d)]. As a consequence, the quality factor loses its double dip structure getting a single dip at $U_{\rm gate} = -eV_{\rm bias}/2$ [solid normal-thickness ($B = 0.2$) and thin ($B = 0.4$) (black) lines in Fig. 9(b)].

We intend now to study the device quality factors as a function of the transverse magnetic field B comparing different conducting states of the device. In Fig. 10(a), one can observe calculated device quality factors as a function of the magnetic field at a low conducting state of the device ($U_{\rm gate} = 0.45$). Different curves, from thicker to thinner, refer to increasing bias voltages applied $eV_{\rm bias} = 0.1$–0.75–1.5. At every fixed bias voltage, a clear quadratic dependence of the total average damping on the magnetic field strength is observed (not shown in Fig. 10), with a Lorentzian shape of the quality factor curves [see Fig. 10(a)]. It is important to point out that the range of magnetic field strengths experimentally investigated in Ref. 1, $B = 0 - 3T$, corresponds to small magnetic fields in our units (we recall that $H_0 = 16.6T$). Remarkably, at low bias and small magnetic fields, a quadratic decrease of the Q against magnetic field is observed [see solid thick (black) line in Fig. 10(a)]. In Fig. 11, we show the quantitative agreement between experimental and calculated quality factors against magnetic field when the device is in a low conducting state, with $eV_{\rm bias} = 0.1$ and $U_{\rm gate} = -0.45$. The slight increase of the quality factor Q as a function of the field for small magnetic fields is due to asymmetry introduced by the gate voltage $U_{\rm gate} = 0.45$ applied to the device [see also Fig. 10(a)]. For gate voltage equal to zero, that in the high conducting state of the device, the calculated Q against B curve is a parabola with a maximum at zero magnetic field applied.

Coming back to Fig. 10(a), one can observe an interesting increase of the quality factor peak as a function of the bias voltage. In particular, for $eV_{\rm bias} = 1.5$ [thinner line in Fig. 10(a)] a quality factor peak at $B \simeq U_{\rm gate}/2 = 0.225$ occurs. This can be directly related to the average total damping dip, not shown in Fig. 10. This effect can be explained noting that, when the bias voltage applied to the electronic device is increased, a transition from a single peak to a double peak structure in the *spatial* dependence total damping affected by the CNT resonator can be observed [compare Figs. 3(a) and 3(d)], while at the same time, the displacement distribution probabilities $P(x)$ spread on the configuration space remain centered at configurations close to the harmonic potential minimum $x \simeq 0$ characteristic of the low bias regime. The overall result is a reduction of the average total damping affecting the CNT resonator whose minimum is translated by a quantity proportional to the gate voltage applied to the device. This argument becomes even more clear when no gate voltage is applied to the device which is therefore placed in a high conducting state. In this case a perfect symmetry of Q-factor curves with respect to zero magnetic field is obtained [see Fig. 10(b)].

We end this section with a study of the device quality factors as a function of the bias voltages and magnetic fields comparing low and high conducting states of the device. In Fig. 10(c), one can observe calculated device quality factors as a function of the bias voltages at a low conducting state of the device ($U_{\rm gate} = 0.45$). Different curves, from thicker to thinner, refer to increasing magnetic field applied to the device $B = 0.0$–0.05–0.1. At zero magnetic field, a clear double dip feature in the quality factor Q, as experimentally observed in Ref. 12, is visible. This can be explained looking at the average total damping and in terms of the average charge

present on the CNT level. The total average damping, in the absence of magnetic field, has two peaks at $eV_{\rm bias} = -2U_{\rm gate} = -0.9$ and at $eV_{\rm bias} = 2U_{\rm gate} = 0.9$. Indeed, as also discussed previously, the total average damping is peaked at electronic configurations where the CNT level experiences half unit charge variations, that is, at $|U_{\rm gate} - eV_{\rm bias}/2| < \hbar\Gamma$ and $|U_{\rm gate} + eV_{\rm bias}/2| < \hbar\Gamma$. Therefore, when the edges of the conduction window (whose width is proportional to $eV_{\rm bias}$) meet the CNT level energy (given by $U_{\rm gate}$), a maximum total average damping (minimum quality factor) is observed. As also discussed in reference to Fig. 9, the double peak structure of the average total damping term is canceled by the magnetic field, giving a single peak at $eV_{\rm bias} = -2U_{\rm gate}$ where a cooperation between negative charge density and positive current variations takes place. As a consequence, the quality factor loses its double dip structure getting a single dip at $eV_{\rm bias} = -2U_{\rm gate}$ [solid normal-thickness ($B = 0.05$) and thin ($B = 0.1$) (black) lines in Fig. 10(c)].

In Fig. 10(d), we show calculated device quality factors as a function of the bias voltages at a high conducting state of the device ($U_{\rm gate} = 0.0$). Different curves, from thicker to thinner, refer to increasing magnetic field applied to the device $B = 0.0$–0.25–0.5. As above, at zero magnetic field, a single dip feature in the quality factor Q, as experimentally observed in Ref. 12, is visible. This behavior can be discussed with the same argument given for discussing Figs. 9(a) and 9(b), where a reduction of the total average damping as a function of the bias voltage applied to the device was observed. Again, a decrease of the quality factor in all the gate voltage range investigated as a function of the magnetic field is observed [see Fig. 10(d)].

V. CONCLUSIONS AND DISCUSSION

In conclusion, we have studied a CNT-based electronic transistor in the presence of an external magnetic field perpendicular to the current flux. The main result is that a magnetic field can be used as a useful tool to tune and probe the mechanical characteristic of the bending mode CNT dynamics. Indeed, a Lorentz-like force acting on the electronic current flowing through the CNT comes into play coupling with the bending mode of the beam itself.

Within our approach, we were able to show that all the terms describing the CNT-resonator dynamics are modified by the external magnetic field. First of all, the total effective force is modified by a pure nonequilibrium correction term proportional to the magnetic field strength as well as to the average electronic current. This provides several interesting resonance frequency renormalization effects. The peculiar (single or double dip) features in the CNT-resonator resonance frequency against gate voltage, obtained in different conducting regimes for the device, get distorted and acquire, in the limit of large magnetic field, a peculiar dip-peak structure that should be experimentally observed. Furthermore, resonance frequencies depend quadratically on the magnetic field strength if the device is a high conducting state, and linearly otherwise.

The transverse magnetic field has been shown to give also an enhanced damping as well as a noise term originating from the electronic phase fluctuations induced by the displacements of CNT itself. In particular, a systematic study of device quality factor as a function of gate and bias voltage in the presence of the magnetic field has also been performed. All results are discussed observing the average charge and electronic current variations with respect to gate voltage applied to the device and can be summarized as follows. At a fixed electronic conducting regime, if negative charge variations and positive current variations occur, one has an enhanced damping reducing the quality factor of the device. Vice versa, negative charge variations and negative current variations reduce damping with a consequent increase of quality factors. Within our model, a quadratic dependence of the device quality factor Q on external magnetic field strength, experimentally observed in Ref. 1, naturally emerges. This behavior is understood in terms of a back-action of quantum electronic current flow fluctuations on the bending mode dynamics.

Finally, when the device is actuated by an external antenna at fixed frequency and amplitude, the device current-gate voltage response is modified by fine structure features any time the mechanical resonance with the proper nanotube oscillation frequency occurs. These structures can be tuned as a function of the external field and could be experimentally observed. In this sense, we have shown that, only exciting the CNT motion with application of an external radio-frequency antenna, one can observe a magnetic field dependence of the electronic current.

We point out that throughout this paper we do not take into account a magnetic field with a component longitudinal to the CNT resonator. This issue has been recently addressed in Ref. 12 and explained in terms of a more sophisticated theoretical schematization of the CNT-resonator electronic structure which has a cylindrical quasi-one-dimensional shape.

We end this section noting that it could be of outstanding interest to study the possibility to include quantum corrections to the oscillator dynamics as well as spin degrees of freedom[34] and electron-electron interaction effects[45] in the low bias regime. In particular, it has been recently proposed to study the CNT bending mode dynamics by employing the spin-orbit coupling between a single spin and nanomechanical displacement[46–48] in the presence of a magnetic field. Quantum corrections becomes important when the resonator and electronic time scales are of the same order on magnitude. In this direction, it was shown in Ref. 33 that a magnetic field applied perpendicular to the CNT results in negative magnetoconductance due to quantum vibrations of the tube inducing an Aharonov-Bohm-like effect[49] on the electrons crossing the device. Work in this direction is in progress.

ACKNOWLEDGMENTS

A.N. acknowledges CNISM for financial support. The research leading to these results has received funding from the FP7/2007-2013 under Grant Agreement No. 264098-MAMA.

APPENDIX A: ADIABATIC APPROXIMATION FOR THE ELECTRON PROBLEM IN THE PRESENCE OF A MAGNETIC FIELD

In this appendix, we show how the adiabatic approximation on the electronic CNT level Green function works in the presence of a transverse magnetic field. Assuming a slow time

dependence of electronic Green functions on the resonator displacement x, we are able to calculate truncated expressions for the CNT level Green functions which acquire a "slow" time dependence and, at first order, a linear correction in the oscillator velocity. As a result of the adiabatic approximation, the truncated CNT level Green functions will depend on the instantaneous value of the position and velocity of the resonator $G^{r,a,<,>}(\omega,x,v)$.

The adiabatic expansion of the Fourier transformed retarded CNT level Green function is

$$G^r(\omega,x,v) = G^r_{(0)}(\omega,x) + G^r_{(1)}(\omega,x,v), \tag{A1}$$

where the expression of $G^r_{(0)}(\omega,x)$ is

$$G^r_{(0)}(\omega,x) = \frac{1}{\hbar\omega - U_{\rm gate}(x) + \imath\hbar\Gamma/2}, \tag{A2}$$

and that of $G^r_{(1)}(\omega,x,v)$ is

$$G^r_{(1)}(\omega,x,v) = \imath\hbar\dot{U}_{\rm gate}(x) G^r_{(0)}(\omega,x)\frac{\partial G^r_{(0)}(\omega,x)}{\partial\hbar\omega}. \tag{A3}$$

Above, $U_{\rm gate}(x) = U_{\rm gate} + \lambda x$ and the dot indicates the time derivative $\dot{U}_{\rm gate} = \lambda\frac{\partial x}{\partial t} = \lambda v$.

Using the adiabatic approximation[34] $x(t_1) - x(t_2) \simeq \dot{x}(t_0)(t_1 - t_2)$, we obtain for the lesser and greater components of the leads' self-energy in Fourier space

$$\Sigma^<_{\rm leads}(\omega,v) \simeq \Sigma^<_{{\rm leads},(0)}(\omega) + \Sigma_{{\rm leads},(1)}(\omega,v), \tag{A4}$$

where the expression of $\Sigma^<_{{\rm leads},(0)}(\omega)$ is

$$\Sigma^<_{{\rm leads},(0)}(\omega) = \imath[\hbar\Gamma_L f_L(\omega) + \hbar\Gamma_R f_R(\omega)], \tag{A5}$$

and that of $\Sigma_{{\rm leads},(1)}(\omega,v)$ is

$$\Sigma_{{\rm leads},(1)}(\omega,v) = -\imath e\tilde{H}\left(\frac{\partial[\hbar\Gamma_L f_L(\omega) + \hbar\Gamma_R f_R(\omega)]}{\partial[eV_{\rm bias}]}\right)v. \tag{A6}$$

Above, we have defined $\tilde{H} = 2p\hbar/e$. The adiabatic correction to the lesser component of the leads' self-energy in Eq. (A6) is entirely due to the transverse magnetic field and represent one of the main results of the present paper, in contrast to previous works where magnetic field effects in the adiabatic expansion were not considered.[16,24,29,30,40]

Definitely, for the CNT level occupation we get

$$\langle\hat{n}\rangle(x,v) \simeq \langle\hat{n}\rangle_{(0)}(x) + \langle\hat{n}\rangle_{(1)}(x,v), \tag{A7}$$

where at zero order in the adiabatic expansion

$$\langle\hat{n}\rangle_{(0)}(x) = \int\frac{d\hbar\omega}{4\pi}[f_L(\omega) + f_R(\omega)]C(\omega,x), \tag{A8}$$

with the spectral function $C(\omega,x) = -2{\rm Im}G^r_{(0)}(\omega,x)$ of the CNT level given by

$$C(\omega,x) = \frac{\hbar\Gamma}{[\hbar\omega - U_{\rm gate}(x)]^2 + [\hbar\Gamma]^2/4}. \tag{A9}$$

The first-order corrections in the adiabatic expansion are linear in the oscillator velocity

$$\langle\hat{n}\rangle_{(1)}(x,v) = v[R_{(1)}(x) + R_{(2)}(x)], \tag{A10}$$

with

$$R_{(1)}(x) = \frac{\lambda}{\Gamma}\int\frac{d\hbar\omega}{2\pi}g^{(1)}_+(\omega)C(\omega,x)T(\omega,x), \tag{A11}$$

$$R_{(2)}(x) = \frac{e\tilde{H}}{2}\int\frac{d\hbar\omega}{2\pi}g^{(2)}_+(\omega)C(\omega,x), \tag{A12}$$

where we have defined the transmission function $T(\omega,x)$

$$T(\omega,x) = \frac{\hbar\Gamma_L\hbar\Gamma_R}{\{[\hbar\omega - U_{\rm gate}(x)]^2 + [\hbar\Gamma]^2/4\}}, \tag{A13}$$

and

$$g^{(1)}_+(\omega) = -\frac{\partial[f_L(\omega) + f_R(\omega)]}{\partial\hbar\omega}, \tag{A14}$$

$$g^{(2)}_+(\omega) = -\frac{\partial[f_L(\omega) + f_R(\omega)]}{\partial[eV_{\rm bias}]}. \tag{A15}$$

Above, $R_{(1)}(x)$ is the the adiabatic correction to the density related to the charge-displacement coupling described in the interaction Hamiltonian Eq. (4), already described in many papers in the literature.[24,29,30] $R_{(2)}(x)$ is the adiabatic correction exclusively due to magnetic-coupling effects modifying the electronic phase of electrons flowing from the leads to the CNT.

Finally, in the hypothesis of symmetric coupling to the leads $\Gamma_L = \Gamma_R$, one can calculate the adiabatic expansion for the symmetrized current $\langle\hat{I}\rangle = [\langle\hat{I}_L\rangle - \langle\hat{I}_R\rangle]/2$,

$$\langle\hat{I}\rangle(x,v) = \frac{e}{\hbar}\int\frac{d\hbar\omega}{2\pi}|G^r(\omega,x)|^2[\Sigma^{R,>}(\omega,v)\Sigma^{L,<}(\omega,v) - \Sigma^{L,>}(\omega,v)\Sigma^{R,<}(\omega,v)]. \tag{A16}$$

Using Eqs. (A1) and (A4), we get

$$\langle\hat{I}\rangle(x,v) \simeq \langle\hat{I}\rangle_{(0)}(x) + \langle\hat{I}\rangle_{(1)}(x,v), \tag{A17}$$

where

$$\langle\hat{I}\rangle_{(0)}(x) = e\Gamma\int\frac{d\hbar\omega}{8\pi}[f_L(\omega) - f_R(\omega)]C(\omega,x), \tag{A18}$$

with linear corrections in the oscillator velocity

$$\langle\hat{I}\rangle_{(1)}(x,v) = v[U_{(1)}(x) + U_{(2)}(x)], \tag{A19}$$

with

$$U_{(1)}(x) = -\frac{e\lambda}{2}\int\frac{d\hbar\omega}{2\pi}g^{(1)}_-(\omega)C(\omega,x)T(\omega,x), \tag{A20}$$

$$U_{(2)}(x) = -\frac{e^2}{\hbar}\tilde{H}\int\frac{d\hbar\omega}{2\pi}g^{(2)}_-(\omega)T(\omega,x), \tag{A21}$$

where we have defined

$$g^{(1)}_-(\omega) = \frac{\partial[f_L(\omega) - f_R(\omega)]}{\partial\hbar\omega}, \tag{A22}$$

$$g^{(2)}_-(\omega) = \frac{\partial[f_L(\omega) - f_R(\omega)]}{\partial[eV_{\rm bias}]}. \tag{A23}$$

As already discussed, referring to adiabatic corrections to the average charge density of the CNT level, $U_{(1)}(x)$ is the the adiabatic correction to the electronic current related to the charge-displacement coupling described in the interaction Hamiltonian Eq. (4), already described in Refs. 26 and 27.

$U_{(2)}(x)$ is the adiabatic correction to the current exclusively due to magnetic-coupling effects. As shown in Sec. III A 1, Eq. (A21) is one of the main results of the present paper, describing the increase of damping acting on the CNT resonator given by the application of a transverse magnetic field.

APPENDIX B: CURRENT-CURRENT AND DENSITY-CURRENT FLUCTUATIONS

In this appendix, we illustrate how the calculation of the force-force fluctuation [Eq. (15)] can be performed with the nonequilibrium Green-function approach. In particular, here we show how one can calculate in the adiabatic approximation the current-current

$$S(t,t') = \langle \delta\hat{I}(t)\delta\hat{I}(t')\rangle \tag{B1}$$

and the density-current

$$M(t,t') = \langle [\delta\hat{n}(t)\delta\hat{I}(t') + \delta\hat{I}(t)\delta\hat{n}(t')]\rangle \tag{B2}$$

fluctuation terms appearing in Eq. (15). Recalling that $\hat{I} = (\hat{I}_L - \hat{I}_R)/2$, it is easy to see that $S(t,t')$ is made of three contributions,

$$S(t,t') = \tfrac{1}{2}[S_L(t,t') + S_R(t,t') + S_{LR}(t,t')], \tag{B3}$$

where

$$S_L(t,t') = \langle \delta\hat{I}_L(t)\delta\hat{I}_L(t')\rangle, \tag{B4}$$

$$S_R(t,t') = \langle \delta\hat{I}_R(t)\delta\hat{I}_R(t')\rangle, \tag{B5}$$

$$S_{LR}(t,t') = -\langle\{\delta\hat{I}_L(t),\delta\hat{I}_R(t')\}\rangle. \tag{B6}$$

The density-current fluctuation term $M(t,t')$ is given by

$$M(t,t') = \tfrac{1}{2}[M_R(t,t') - M_L(t,t')], \tag{B7}$$

where

$$M_L(t,t') = \langle\{\delta\hat{I}_L(t),\delta\hat{n}(t')\}\rangle, \tag{B8}$$

$$M_R(t,t') = \langle\{\delta\hat{I}_R(t),\delta\hat{n}(t')\}\rangle. \tag{B9}$$

Above, $\{A,B\} = AB + BA$ is an anticommutator. In this appendix we limit to calculate $S_L(t,t')$ and $M_L(t,t')$ in the adiabatic approximation, since for the other fluctuation terms the derivation is similar.

We recall the expression for the current operator (through the left barrier),[50]

$$I_L = \frac{\imath e}{\hbar}\sum_k [V_{L,k}c_k^\dagger d - V_{L,k}^* d^\dagger c_k]. \tag{B10}$$

We define $\delta\hat{I}_L(t) = \hat{I}_L(t) - \langle\hat{I}_L\rangle$, and plan to evaluate the correlation function (we set $V_{L,k} = V_k$),

$$\begin{aligned} S_L(t,t') &= \frac{1}{2}\langle\{\delta\hat{I}_L(t),\delta\hat{I}_L(t')\}\rangle \\ &= \frac{1}{2}\langle\{I_L(t),I_L(t')\}\rangle - \langle\hat{I}_L\rangle^2 \\ &= \frac{1}{2}\left(\frac{\imath e}{\hbar}\right)^2\sum_{k,k'}[V_kV_{k'}\langle c_k^\dagger(t)d(t)c_{k'}^\dagger(t')d(t')\rangle \\ &\quad - V_kV_{k'}^*\langle c_k^\dagger(t)d(t)d^\dagger(t')c_{k'}(t')\rangle \\ &\quad - V_k^*V_{k'}\langle d^\dagger(t)c_k(t)c_{k'}^\dagger(t')d(t')\rangle \\ &\quad + V_k^*V_{k'}^*\langle d^\dagger(t)c_k(t)d^\dagger(t')c_{k'}(t')\rangle] + \text{H.c.} - \langle\hat{I}_L\rangle^2. \end{aligned} \tag{B11}$$

The Fourier transform of S is called the noise spectrum; in what follows we shall be particularly concerned with its zero-frequency component, $S(0) = \int d(t-t')S(t-t')$, that is, the relevant quantity in the adiabatic expansion. In order to evaluate the (nonequilibrium) expectation values occurring in Eq. (B11) in a systematic way, we first define the following contour-ordered two-particle Green functions (we follow Ref. 50),

$$\begin{aligned} G_1^{cd}(\tau,\tau') &= \imath^2\langle T_C c_k^\dagger(\tau)d(\tau)c_{k'}^\dagger(\tau')d(\tau')\rangle, \\ G_2^{cd}(\tau,\tau') &= \imath^2\langle T_C c_k^\dagger(\tau)d(\tau)d^\dagger(\tau')c_{k'}(\tau')\rangle, \\ G_3^{cd}(\tau,\tau') &= \imath^2\langle T_C d^\dagger(\tau)c_k(\tau)c_{k'}^\dagger(\tau')d(\tau')\rangle, \\ G_4^{cd}(\tau,\tau') &= \imath^2\langle T_C d^\dagger(\tau)c_k(\tau)d^\dagger(\tau')c_{k'}(\tau')\rangle. \end{aligned} \tag{B12}$$

The nonequilibrium noise correlator is then given by

$$\begin{aligned} S_L(t,t') = \frac{1}{2}\left(\frac{e}{\hbar}\right)^2\sum_{k,k'}&[V_kV_{k'}G_1^{cd,>}(t,t') \\ &- V_kV_{k'}^*G_2^{cd,>}(t,t') - V_k^*V_{k'}G_3^{cd,>}(t,t') \\ &+ V_k^*V_{k'}^*G_4^{cd,>}(t,t')] + \text{H.c.} - \langle\hat{I}_L\rangle^2, \end{aligned} \tag{B13}$$

where $G_i^{cd,>}(t,t')$ are the greater-than components of the contour-ordered counterparts $G_i^{cd}(\tau,\tau')$ defined in Eq. (B12). In the adiabatic approximation, we consider the zero-order terms of all Green functions G. After lengthy but straightforward calculations, starting from Eq. (B13) we get (we follow Ref. 50)

$$\begin{aligned} S(t,t') &= [S_L(t,t') + S_R(t,t') + S_{LR}(t,t')]/2 \\ &= D^H(x)\delta(t-t'), \end{aligned} \tag{B14}$$

where $D^H(x)$ is given by Eq. (20) of the main text. Equation (20) is a well-known, and important, result. The first term accounts for thermal noise (i.e., it vanishes at zero temperature), while the second term is a nonequilibrium term (shot noise), which vanishes at zero bias.

For the mixed current-density contribution in the second line of Eq. (15), we have (for the left lead)

$$\begin{aligned} M_L(t,t') &= \langle\{\delta I_L(t),\delta n(t')\}\rangle \\ &= \langle\{I_L(t),n(t')\}\rangle - 2\langle\hat{I}_L\rangle^2\langle\hat{n}\rangle^2 \\ &= \frac{\imath e}{\hbar}\sum_{k_L}\left[V_{k_L}\left\langle c_{k_L}^\dagger(t)d(t)d^\dagger(t')d(t')\right\rangle\right. \\ &\quad \left. - V_{k_L}^*\left\langle d^\dagger(t)c_{k_L}(t)d^\dagger(t')d(t')\right\rangle\right] + \text{H.c.} \\ &\quad - 2\langle\hat{I}_L\rangle^2\langle\hat{n}\rangle^2. \end{aligned} \tag{B15}$$

As for the the current noise spectrum S, in what follows we shall be particularly concerned with the zero-frequency component of $M_L(t,t')$, $M_L(\omega=0) = \int d(t-t')M_L(t-t')$, that is, the relevant quantity in the adiabatic expansion. In order to evaluate the (nonequilibrium) expectation values occurring

in Eq. (B15) in a systematic way, we first define the following contour-ordered two-particle Green functions:

$$G^{Mcd}_{1,L}(\tau,\tau') = \imath^2\langle T_C c^\dagger_{k_L}(\tau)d(\tau)d^\dagger(\tau')d(\tau')\rangle,$$
$$G^{Mcd}_{2,L}(\tau,\tau') = \imath^2\langle T_C d^\dagger(\tau)c_{k_L}(\tau)d^\dagger(\tau')d(\tau')\rangle. \quad \text{(B16)}$$

In terms of the previous Green function in Eq. (B16), The nonequilibrium current-density noise correlator M is then given by

$$M_L(t,t') = \frac{\imath e}{\hbar}\sum_{k_L}\left[V_{k_L}G^{Mcd,>}_{1,L}(t,t') - V^*_{k_L}G^{Mcd,>}_{2,L}(t,t')\right] + \text{H.c.} - 2\langle I_L\rangle^2\langle\hat{n}\rangle^2, \quad \text{(B17)}$$

where $G^{Mcd,>}_{i,L}(t,t')$ are the greater-than components of the contour-ordered counterparts $G^{Mcd}_{i,L}(\tau,\tau')$ defined in Eq. (B16). Following the same reasoning as in the previous section, one can show that

$$M_L(t,t') \simeq \frac{e}{\hbar}\left\{G^>(t,t')\left[\int_C d\tau_1 G(t,\tau_1)\Sigma_L(\tau_1,t')\right]^< - G^<(t',t)\left[\int_C d\tau_1\Sigma_L(t,\tau_1)G(\tau_1,t')\right]^> + G^<(t,t')\left[\int_C d\tau_1 G(t,t_1)\Sigma_L(\tau_1,t')\right]^> - G^>(t',t)\left[\int_C d\tau_1\Sigma_L(t,\tau_1)G(\tau_1,t')\right]^<\right\}, \quad \text{(B18)}$$

where Σ_L is the self-energy contribution due to the coupling to the left lead and the integration is extended along the Keldysh contour. The function

$$f(t,t') = \left[\int_C d\tau_1 G(t,\tau_1)\Sigma_L(\tau_1,t')\right]^< \quad \text{(B19)}$$

can be calculated using Langreth's rules,[50] giving

$$f(t,t') = \int dt_1 G^r(t,t_1)\Sigma^<_L(t_1,t') + G^<(t,t_1)\Sigma^a_L(t_1,t'), \quad \text{(B20)}$$

where Σ^a_L is the advanced component of the left lead self-energy. In the adiabatic approximation, we consider the zero-order terms of all functions G and Σ. After lengthy but straightforward calculations, starting from Eq. (B18) we get

$$M(t,t') = [M_R(t,t') - M_L(t,t')]/2 = D^{H\lambda}(x)\delta(t-t'), \quad \text{(B21)}$$

where $D^{H\lambda}(x)$ is given by Eq. (19).

[1] D. R. Schmid, P. L. Stiller, Ch. Strunk, A. K. Huettel, New J. Phys. **14**, 083024 (2012).
[2] G. A. Steele, A. K. Huttel, B. Witkamp, M. Poot, H. B. Meerwaldt, L. P. Kouwenhoven, and H. S. J. van der Zant, Science **325**, 1103 (2009).
[3] A. K. Huttel, G. A. Steele, B. Witkamp, M. Poot, L. P. Kouwenhoven, and H. S. J. van der Zant, Nano Lett. **9**, 2547 (2009).
[4] A. Castellanos-Gomez, H. B. Meerwaldt, W. J. Venstra, H. S. J. van der Zant, and G. A. Steele, Phys. Rev. B **86**, 041402(R) (2012).
[5] A. Eichler, M. del Alamo Ruiz, J. A. Plaza, and A. Bachtold, Phys. Rev. Lett. **109**, 025503 (2012).
[6] B. J. LeRoy, I. Heller, V. K. Pahilwani, C. Dekker, and S. G. Lemay, Nano Lett. **7**, 2937 (2007).
[7] N. Traverso Ziani, G. Piovano, F. Cavaliere, and M. Sassetti, Phys. Rev. B **84**, 155423 (2011); N. Traverso Ziani, F. Cavaliere, G. Piovano, and M. Sassetti, Phys. Scr. **T151**, 014041 (2012); G. Piovano, F. Cavaliere, E. Paladino, and M. Sassetti, Phys. Rev. B **83**, 245311 (2011).
[8] F. Cavaliere, E. Mariani, R. Leturcq, C. Stampfer, and M. Sassetti, Phys. Rev. B **81**, 201303 (2010).
[9] J. O. Island, V. Tayari, A. C. McRae, and A. R. Champagne, Nano Lett. **12**, 4564 (2012).
[10] B. H. Schneider, S. Etaki, H. S. J. van der Zant, and G. A. Steele, Sci. Rep. **2**, 599 (2012); A. D. O'Connell, M. Hofheinz, M. Ansmann, R. C. Bialczak, M. Lenander, E. Lucero, M. Neeley, D. Sank, H. Wang, M. Weides, J. Wenner, J. M. Martinis, and A. N. Cleland, Nature **464**, 697 (2010).
[11] B. Witkamp, M. Poot, and H. S. J. van der Zant, Nano Lett. **6**, 2904 (2006).
[12] H. B. Meerwaldt, G. Labadze, B. H. Schneider, A. Taspinar, Y. M. Blanter, H. S. J. van der Zant, and G. A. Steele, Phys. Rev. B **86**, 115454 (2012).
[13] D. H. Cobden and J. Nygard, Phys. Rev. Lett. **89**, 046803 (2002).
[14] M. Bockrath, D. H. Cobden, P. L. McEuen, N. G. Chopra, A. Zettl, A. Thess, and R. E. Smalley, Science **725**, 1922 (1997).
[15] S. J. Tans, M. H. Devoret, H. Dai, A. Thess, R. E. Smalley, L. J. Geerligs, and C. Dekker, Nature (London) **386**, 474 (1997).
[16] A. Nocera, C. A. Perroni, V. Marigliano Ramaglia, and V. Cataudella, Phys. Rev. B **86**, 035420 (2012).
[17] G. Labadze and Ya. M. Blanter, arXiv:1007.5186v2 [cond-mat.mes-hall].
[18] Ya. M. Blanter, O. Usmani, and Yu. V. Nazarov, Phys. Rev. Lett. **93**, 136802 (2004).
[19] Ya. M. Blanter, O. Usmani, and Yu. V. Nazarov, Phys. Rev. Lett. **94**, 049904(E) (2005).
[20] H. B. Meerwaldt, G. A. Steele, and H. S. J. van der Zant, *Fluctuating Nonlinear Oscillators: From Nanomechanics to Quantum Superconducting Circuits* (Oxford University Press, Oxford, 2012), p. 312.
[21] G. Weick and Dominique M.-A. Meyer, Phys. Rev. B **84**, 125454 (2011).
[22] Here, the quantum regime effects predicted in Refs. 33 and 23 are not relevant due to the very low ratio between the CNT bending-mode energy and the tunneling energy to the leads.
[23] G. Rastelli, M. Houzet, and F. Pistolesi, Europhys. Lett. **89**, 57003 (2010).
[24] A. Nocera, C. A. Perroni, V. Marigliano Ramaglia, and V. Cataudella, Phys. Rev. B **83**, 115420 (2011).

[25]J. Splettstoesser, M. Governale, J. Konig, and R. Fazio, Phys. Rev. Lett. **95**, 246803 (2005).
[26]N. Bode, S. V. Kusminskiy, R. Egger, and F. von Oppen, Phys. Rev. Lett. **107**, 036804 (2011).
[27]N. Bode, S. V. Kusminskiy, R. Egger, and F. von Oppen, Beilstein J. Nanotechnol. **3**, 144 (2012).
[28]A. Metelmann and T. Brandes, Phys. Rev. B **84**, 155455 (2011).
[29]F. Pistolesi, Ya. M. Blanter, and I. Martin, Phys. Rev. B **78**, 085127 (2008).
[30]R. Hussein, A. Metelmann, P. Zedler, and T. Brandes, Phys. Rev. B **82**, 165406 (2010).
[31]In Ref. 32, the authors consider the presence of a Laplace force analogous to that derived by us and a cohesive force acting on the resonator in the presence of an external transverse magnetic field. As suggested in Ref. 32, one can safely neglect the cohesive force effects if $H \gg l/L H_0^*$, where H_0^* is a characteristic magnetic field, l is the distance of the quantum dot from the leads, and L is the CNT length. In our schematization $l \ll L$, since we reduce the entire CNT as a quantum dot attached to the leads. Therefore, we can safely neglect the cohesive force effects.
[32]G. A. Skorobagatko, S. I. Kulinich, I. V. Krive, R. I. Shekhter, and M. Jonson, Low Temp. Phys. **37**, 1032 (2011).
[33]R. I. Shekhter, L. Y. Gorelik, L. I. Glazman, and M. Jonson, Phys. Rev. Lett. **97**, 156801 (2006).
[34]D. Radic, A. Nordenfelt, A. M. Kadigrobov, R. I. Shekhter, M. Jonson, and L. Y. Gorelik, Phys. Rev. Lett. **107**, 236802 (2011).
[35]G. Rastelli, M. Houzet, L. I. Glazman, and F. Pistolesi, C. R. Phys. **13**, 410 (2012).
[36]F. Romeo and R. Citro, Phys. Rev. B **80**, 235328 (2009).
[37]G. Weick, F. von Oppen, and F. Pistolesi, Phys. Rev. B **83**, 035420 (2011).
[38]A. D. Armour, M. P. Blencowe, and Y. Zhang, Phys. Rev. B **69**, 125313 (2004).
[39]Actually, more sophisticated approaches involving the coupling with spatial fluctuations of the CNT electronic density, recently proposed in Refs. 7 and 8, are not needed in the present case, but are very important to describe scanning tunnel microscopy experiments performed on suspended CNTs (Ref. 6).
[40]D. Mozyrsky, M. B. Hastings, and I. Martin, Phys. Rev. B **73**, 035104 (2006).
[41]C. A. Perroni, A. Nocera, V. M. Ramaglia, and V. Cataudella, Phys. Rev. B **83**, 245107 (2011); C. A. Perroni, V. Marigliano Ramaglia, and V. Cataudella, *ibid.* **84**, 014303 (2011).
[42]F. Gargiulo, C. A. Perroni, V. M. Ramaglia, and V. Cataudella, Phys. Rev. B **84**, 245204 (2011); V. Cataudella, G. De Filippis, and C. A. Perroni, *ibid.* **83**, 165203 (2011).
[43]C. A. Perroni and V. Cataudella, Phys. Rev. B **85**, 155205 (2012); Europhys. Lett. **98**, 47004 (2012).
[44]In the large bias regime, features of different origin than those investigated in this paper can appear in the current-voltages characteristic of the device. These switching effects are experimentally observed in dc current through the device investigated in Ref. 1, and have been identified as nanoelectromechanical self-excitations of the system, where positive feedback from single electron tunneling drives mechanical motion. These features, smeared by the external magnetic field, were predicted by a model introduced in Refs. 18 and 19 where energy dependence of electronic tunneling amplitudes was also considered.
[45]V. V. Deshpande, M. Bockrath, L. I. Glazman, and A. Yacoby, Nature (London) **464**, 209 (2010); V. V. Deshpande and M. Bockrath, Nat. Phys. **4**, 314 (2008); F. Cavaliere, U. De Giovannini, M. Sassetti, and B. Kramer, New J. Phys. **11**, 123004 (2009).
[46]C. Ohm, C. Stampfer, J. Splettstoesser, and M. R. Wegewijs, Appl. Phys. Lett. **100**, 143103 (2012).
[47]A. Palyi, P. R. Struck, M. Rudner, K. Flensberg, and G. Burkard, Phys. Rev. Lett. **108**, 206811 (2012); M. S. Rudner and E. I. Rashba, Phys. Rev. B **81**, 125426 (2010).
[48]C. A. Perroni and A. Liebsch, Phys. Rev. B **74**, 134430 (2006).
[49]When an electron crosses the device, its wave function acquires an Aharonov-Bohm phase that depends on the position of the displaced oscillator (see Fig. 1 for a schematic representation of the system). The total transmission results from the interference of all electronic trajectories. Thus the Aharonov-Bohm phases generate a magnetic field dependence of the current that is absent, as we show in this paper, in the case of a single classical path.
[50]H. Haug and A.-P. Jauho, *Quantum Kinetics in Transport and Optics of Semiconductors* (Springer, Berlin, 2008).